Exploiting interfacial and size effects to construct oxide superlattices with robust and tunable magnetoelectric properties at room temperature

Yurong Yang,[1] L. Bellaiche,[1] and Jorge Íñiguez[2,3]

[1]*Physics Department and Institute for Nanoscience and Engineering, University of Arkansas, Fayetteville, Arkansas 72701, USA*

[2]*Institut de Ciència de Materials de Barcelona (ICMAB-CSIC), Campus UAB, E-08193 Bellaterra, Spain*

[3]*Materials Research and Technology Department, Luxembourg Institute of Science and Technology, 5 avenue des Hauts-Fourneaux, L-4362 Esch/Alzette, Luxembourg*

(Received 8 September 2014; revised manuscript received 4 February 2015; published 23 February 2015)

We propose a strategy to create materials displaying robust and tunable magnetoelectric multiferroic properties at room temperature. The key idea is to construct heterostructures that combine two different constituents: (1) compound $BiFeO_3$, which presents strong ferroelectric and antiferromagnetic orders well above room temperature, but displays a small magnetic moment, and (2) a ferromagnetic insulator (e.g., $BiMnO_3$) that is only required to couple magnetically with $BiFeO_3$. Our simulations show that it is possible to combine such materials to create superlattices that present (i) a room-temperature multiferroic state with relatively large magnetization (up to $0.3\mu_B$ per transition metal atom, with the possibility to improve by finding a suitable replacement for $BiMnO_3$), (ii) an amply customizable magnetic behavior, and (iii) a strong magnetoelectric coupling. Thus, the design strategy successfully addresses a great challenge in the area of magnetoelectric multiferroics, exploiting interfacial couplings and size (layer-thickness) effects to produce materials apt for applications.

DOI: 10.1103/PhysRevB.91.075423 PACS number(s): 77.55.Nv, 68.65.Cd, 75.50.Dd, 75.70.Cn

I. INTRODUCTION

From an applications perspective, the requirements for an ideal magnetoelectric multiferroic (MEM) material are large values of the polarization and magnetization at room temperature, a strong coupling between the electric and magnetic orders, and good insulating properties. As regards the all-important family of ABO_3 perovskite oxides, the difficulties to find materials that present all these features simultaneously have been discussed [1–3]. Today, the most robust room-temperature multiferroics are materials such as $BiFeO_3$ (BFO) [4], where magnetism is associated with the Fe^{3+} cations located at the B site of the lattice, while ferroelectricity is driven by the off centering of the A-site Bi^{3+} cations.

The simple ABO_3 perovskites displaying room-temperature multiferroism tend to have an antiferromagnetic (AFM) structure; in some cases, the AFM order is modulated, and in others it presents a spin canting that gives rise to a small magnetic moment (e.g., about $0.01\mu_B$ per Fe cation in AFM thin films of BFO) [5–7]. Large magnetization values are unheard of in this context, for fundamental reasons: MEM perovskite oxides are insulators in which the dominant magnetic interaction is superexchange. While AFM superexchange can be very strong (e.g., BFO's Néel temperature is $T_N = 643$ K) [8], ferromagnetic (FM) superexchange is rare and relatively weak [9], a fact that explains the paucity of insulators that present large FM moments at room temperature. Among the most promising materials, it is worth noting $BiMnO_3$ (BMO, with $T_C = 105$ K) [10] or more complex double perovskites such as La_2MnNiO_6 ($T_C = 275$ K) [11,12]. Interestingly, for some time BMO was believed to be a MEM, although its paraelectric character ($C2/c$ space group) is now accepted [13]. La_2MnNiO_6 is paraelectric as well; nevertheless, a strategy to induce a small (improper) polarization in it, and thus obtain a near-room-temperature MEM, has recently been proposed [14]. Higher magnetic Curie temperatures have been predicted for perovskite oxides involving $5d$ transition metals (e.g., $T_C = 360$ K for Bi_2NiReO_6) [15], but such an increase is unfortunately accompanied by a deterioration of the insulating character; the increased spread of the d orbitals results in stronger magnetic couplings, but also closes the gap. Hence, the materials-design challenge remains open.

Here we propose an appealing solution to this problem. As others before us [16–19], we want to take advantage of possibilities provided by artificial heterostructures, introducing a design concept that is likely to yield large and robust MEM effects at room temperature. The basic idea is to create heterostructures combining a high-T_N^{bulk} antiferromagnet with a lower-T_C^{bulk} FM insulator, as sketched in Fig. 1(a) for the case of a superlattice (SL) geometry. By choosing the stacking direction parallel to the $\boldsymbol{q}$ vector characterizing the AFM order, we can construct an artificial material with a well-defined magnetic ground state. As shown in Fig. 1(a), the magnetization will be dominated by the contribution of the FM layers, provided they are thick enough. For thick enough AFM layers, we will have a magnetic ordering transition at T_t close to T_N^{bulk}. Due to the exchange interactions across the interface, the FM layers can be expected to be partly ordered above T_C^{bulk}; therefore, we might have a sizable magnetization $M(T) \neq 0$ for $T > T_C^{bulk}$. (Note that proximity and size effects of this kind are typical of magnetic superlattices and bilayers [20,21].) Furthermore, ferroelectricity can be effectively induced in a SL structure, e.g., by inserting strongly ferroelectric (FE) layers or by means of epitaxial strain [22,23]. Hence, as a result, this design concept can potentially lead to large MEM effects at room temperature, as we will indeed show in the following. Here we demonstrate, for BFO:BMO superlattices grown along the pseudocubic [111] direction, that this strategy can indeed work. Moreover, the analysis of the results for BFO:BMO naturally indicates that other superlattices combining a high-T_N^{bulk} antiferromagnet and a lower-T_C^{bulk} FM insulator should give similar behaviors.

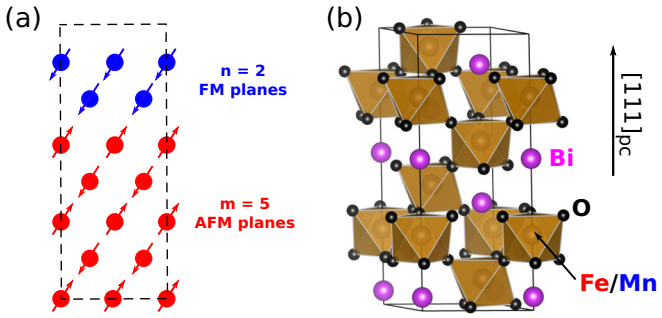

FIG. 1. (Color online) (a) Sketch of a superlattice with AFM (red) and FM (blue) layers that couple antiferromagnetically across the interface. We indicate the ground-state spin configuration, which corresponds to a periodic repetition of the indicated cell provided that the number of planes in the AFM layer m is odd. (b) Basic 30-atom cell corresponding to the hexagonal representation of BFO's $R3c$ phase. Note that this cell can be taken as a $(111)_{pc}$-oriented unit with six atomic planes in it; this structure was the starting point to construct all the superlattices investigated from first principles in this work.

II. METHODS

For the electronic structure calculations, we used density functional theory (DFT) within the local-density approximation (LDA), as implemented in the VASP simulation package [24,25] including a Hubbard U correction [26] for a better treatment of the $3d$ electrons of the transition metal atoms. More specifically, we used U values of 3.8 and 5.3 eV, respectively, for the Fe and Mn cations; these are standard choices that are known to produce qualitatively and quasi-quantitatively correct results for these compounds [27,28]. We used the projector augmented method to represent the ionic cores [25,29], treating explicitly the electrons in the following atomic orbitals: $3p$, $3d$, and $4s$ for both Fe and Mn; Bi's $5d$, $6s$, and $6p$; and O's $2s$ and $2p$. We represented the electronic wave functions in a basis of plane waves cut off at 550 eV. We used a basic 30-atom cell defined by the following lattice vectors: $\boldsymbol{a} = a(\boldsymbol{x}_1 - \boldsymbol{x}_2)$, $\boldsymbol{b} = a(\boldsymbol{x}_2 - \boldsymbol{x}_3)$, and $\boldsymbol{c} = 2a(\boldsymbol{x}_1 + \boldsymbol{x}_2 + \boldsymbol{x}_3)$, where a is the lattice parameter of the elementary pseudocubic five-atom perovskite cell and $\boldsymbol{x}_1$, $\boldsymbol{x}_2$, and $\boldsymbol{x}_3$ are unit vectors along the $[100]_{pc}$, $[010]_{pc}$, and $[001]_{pc}$ pseudocubic directions, respectively. Note that this is the conventional cell of the $R3c$ phase of BFO in the hexagonal setting, which is perfectly adapted to describe a $(111)_{pc}$-oriented superlattice with the third lattice vector $\boldsymbol{c}$ along the stacking direction z. In our first-principles simulations, we have always considered either this cell [sketched in Fig. 1(b)] or a multiple of it along z. The corresponding Brillouin zone integrals have been computed using a $5 \times 5 \times 2$ k-point grid. Structural relaxations were stopped when the residual forces went below 0.001 eV/Å.

We computed the electric polarizations within a linear approximation, using the corresponding dynamical charge tensors as obtained from first principles for each of the considered ferroelectric (FE) structures. We quantified the polar distortion by using as a reference a centrosymmetric (cubiclike) structure that has the (distorted) cell of the FE configuration. As shown below, this procedure tends to underestimate the polarization computed directly from first principles using the Berry's phase formalism, yet it allows us to obtain qualitatively correct results in a fast and reliable way.

For our statistical investigations of the magnetic properties of the superlattices (SLs), we used the simple spin model described in the main text [see Eq. (1)]. We computed the exchange constants by requesting that the model reproduces the first-principles energies obtained for representative spin configurations (in essence, FM and G-AFM). Then, we solved our spin Hamiltonians by means of standard Metropolis Monte Carlo techniques, using a periodically repeated supercell that contains $24 \times 24 \times 24$ elementary perovskite cells. Note that, while this supercell is pseudocubic, it is nevertheless able to capture the $(111)_{pc}$-oriented SLs we want to investigate, provided the chemical layering along the $[111]_{pc}$ direction is properly introduced in the simulation. In our Monte Carlo runs, we typically used 40 000 sweeps for thermalization and 60 000 additional sweeps for computing statistical averages.

III. RESULTS

A. Basic features and ferroelectricity

As indicated above, we choose BFO (high-T AFM and FE) and BMO (FM) as representative and convenient materials to form our superlattices. Note that BFO thin films present a so-called G-AFM structure with nearest-neighboring spins lying antiparallel to each other [5,6]. Such an ordering is characterized by the $\boldsymbol{q} = \pi/a(1,1,1)$ modulation vector, where a is the lattice parameter of the five-atom pseudocubic perovskite cell. Hence, we build our SLs along the $[111]_{pc}$ pseudocubic direction (z in the following), and use for the simulations the basic cell shown in Fig. 1(b). Interestingly, it should be relatively easy to grow BFO:BMO SLs along $[111]_{pc}$, since (1) a variety of BFO-BMO compounds have already been synthesized [28,30], likely because BMO layers can adopt a $R3c$-like structure [28] having a small lattice constant mismatch of 0.4% compared to the $R3c$ state of pure BFO, (2) $(111)_{pc}$-oriented BFO thin films have also been successfully grown (on a $SrRuO_3$ substrate) [31,32], and (3) substrates different from $SrRuO_3$ but still providing a moderate epitaxial strain can also stabilize the rhombohedral-like structure in the BFO:BMO SLs.

We first ran structural relaxations to investigate the basic features of these $(111)_{pc}$-oriented $(BFO)_m$:$(BMO)_n$ SLs. For most of our exploratory simulations we considered a $(BFO)_3$:$(BMO)_3$ superlattice. In all our optimizations, we took as the starting point the structure of BFO's $R3c$ FE phase which displays a spontaneous polarization $\boldsymbol{P}$ along one of the eight $\langle 111\rangle_{pc}$ directions. Because of the $t_{2g}^3 e_g^1$ electronic configuration of Mn^{3+}, in the relaxed SLs the oxygen octahedra containing Mn^{3+} cations are Jahn-Teller distorted, with a splitting between long, medium, and short O-Mn-O bonding distances that is characteristic of many manganese perovskite oxides. When constructing our SLs, we can choose the polar distortion to be parallel to the stacking direction z (i.e., $\boldsymbol{P} \parallel \pm[111]_{pc}$) or to form a 71° (equivalently, 109°) angle with it (i.e., we have the symmetry-related cases with $\boldsymbol{P} \parallel \pm[\bar{1}11]_{pc}$, $\boldsymbol{P} \parallel \pm[1\bar{1}1]_{pc}$, or $\boldsymbol{P} \parallel \pm[11\bar{1}]_{pc}$). We consid-

ered representative cases for both alternatives, and observed the following common ferroelectric features.

All considered SLs are insulating, with the BMO layers adopting a FE distortion that closely resembles that of BFO. Note that BMO layers could become paraelectric (i.e., adopt a structure similar to the $C2/c$ space group of bulk BMO) when they are very thick; this is why here we work with relatively thin BMO layers. We can estimate the polarization from the atomic structural distortions and corresponding Born charges. For the SL with $\boldsymbol{P} \parallel z$ we got 0.58 C/m^2, to be compared with the value of 0.63 C/m^2 obtained for bulk BFO within the same approximation. (Note that the Berry phase result for BFO is 0.91 C/m^2, which suggests that our approximate and computationally convenient scheme to estimate $\boldsymbol{P}$ tends to render relatively small values.) We can further estimate the polarization of the different layers. For the $\boldsymbol{P} \parallel z$ case we get 0.61 C/m^2 for BFO and 0.55 C/m^2 for BMO, which is indicative of a rather homogeneous polar distortion. As regards the SLs with $\boldsymbol{P}$ oblique to z, we get an in-plane polarization of 0.56 C/m^2 (0.59 and 0.54 C/m^2 for BFO and BMO layers, respectively) and an out-of-plane component of 0.21 C/m^2 (0.20 C/m^2 for BFO and 0.22 C/m^2 for BMO). Further, for thick enough BFO layers we can expect the BFO:BMO SLs to have a high FE Curie temperature approaching that of BFO.

Our calculations indicate that it is energetically favorable for the polar distortion to have an in-plane component and thus form an oblique angle with z. The computed energy splitting between the oblique-to-z and parallel-to-z cases is 8.4 meV per five-atom cell for the 3:3 SL. Hence, in the following we will give quantitative results for this energetically preferred situation.

B. Tunable magnetic behavior

To investigate the magnetic interactions in our SLs, we assumed a simple spin Hamiltonian of the form

$$E - E_0 = \frac{1}{2N} \sum_{i \neq j} J_{ij} \boldsymbol{S}_i \cdot \boldsymbol{S}_i, \qquad (1)$$

where E_0 is a reference energy, i and j label five-atom cells, the sum is restricted to first-nearest-neighboring cells, and N is the number of cells in a periodically repeated supercell. For simplicity, we assume classical spins and take $|\boldsymbol{S}_i| = 1$ for the calculation of the exchange constants. [Nominally, the Fe^{3+} cations have a magnetic moment of 5 Bohr magnetons (μ_B) associated with them, while the Mn^{3+} cations present 4μ_B.] In the SLs, the Mn-Mn interactions within the BMO layers are FM in character. The Fe-Fe interactions within the BFO layers are AFM in character. The Mn-Fe interactions at the interface are AFM in character. By computing the energies of different spin arrangements, using our DFT+U scheme, the exchange constants can be obtained [14].

The computed exchange constants between first-nearest-neighboring magnetic atoms in the $(BFO)_3$:$(BMO)_3$ SL are $J_{FeFe} = 44.2$ meV, $J_{MnMn} = -20.0$ meV, and $J_{FeMn} = 20.1$ meV. We computed the analogous magnetic couplings for other $(BFO)_m$:$(BMO)_n$ (m:n) systems. As shown in Fig. 2, J_{FeFe}, J_{MnMn}, and J_{FeMn} for different SLs have very similar values. One can see that the J_{FeFe} exchange constant in the SLs is very close to the corresponding one in BFO bulk (46.2 meV), while J_{MnMn} in SLs is slightly higher in magnitude than that in BMO bulk with $C2/c$ symmetry (−16 meV) and Cc symmetry (−16.6 meV, obtained using a BFO-like structure that is Jahn-Teller distorted). We also calculated the Mn-Fe coupling in a hypothetical Bi_2FeMnO_6 double perovskite with a BFO-like structure, to obtain $J_{FeMn} = 8.5$ meV. Hence, we will use a fixed set of exchange interactions between first-neighboring pairs to investigate $(BFO)_m$:$(BMO)_n$ SLs with arbitrary m:n stacking. We solved the corresponding spin Hamiltonians by means of Monte Carlo (MC) simulations [33].

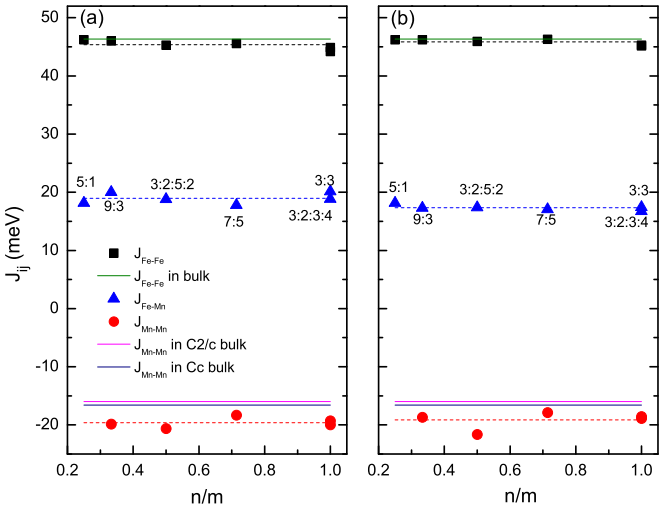

FIG. 2. (Color online) Magnetic exchange constants J_{ij} as a function of the n/m ratio for the $(BFO)_m$:$(BMO)_n$ and $(BFO)_{m_1}$:$(BMO)_{n_1}$:$(BFO)_{m_2}$:$(BMO)_{n_2}$ (with $n_1 + n_2 = n$ and $m_1 + m_2 = m$) superlattices having an electrical polarization pointing along (a) the $[11\bar{1}]$ pseudocubic direction and (b) the [111] pseudocubic direction. The values of the exchange constants used in our simulations are indicated by dashed lines. The exchange constant in BFO bulk (in its $R3c$ ground state) and in BMO bulk (both in the $C2/c$ and Cc states) are also displayed by means of solid horizontal lines, for comparison.

Figure 3(a) shows the obtained results for the magnetic ordering transition temperature (T_t), which evidence two clear trends. First, the thickness of the BFO layers is the main factor controlling T_t, which ranges from about 350 K for $m = 3$ to values approaching the transition temperature of bulk BFO (643 K) for large m. Second, for a given value of m, the transition temperature increases as the thickness of the BMO layers n decreases. This is a rather natural result given that the Mn cations have relatively weak exchange couplings associated with them, and their presence results in an effective reduction of the dimensionality of the spin order within the BFO layers. It is worth noticing that T_t of all the superlattices is largely enhanced with respect to the Curie temperature of BMO bulk ($T_C = 105$ K). In particular, the transition temperature is above room temperature for superlattices with $m > 1$.

Figure 3(b) shows the magnetization of these SLs, $M(T)$, as computed at 200, 250, and 300 K (T_{room}), one of the key quantities we would like to optimize. As in the case of T_t, the results are strongly SL dependent, and some general trends can be observed. For example, the largest M values at the lowest T shown (200 K) correspond to the SLs with thickest BMO layers (see results for $n/m > 1.25$). In such cases we

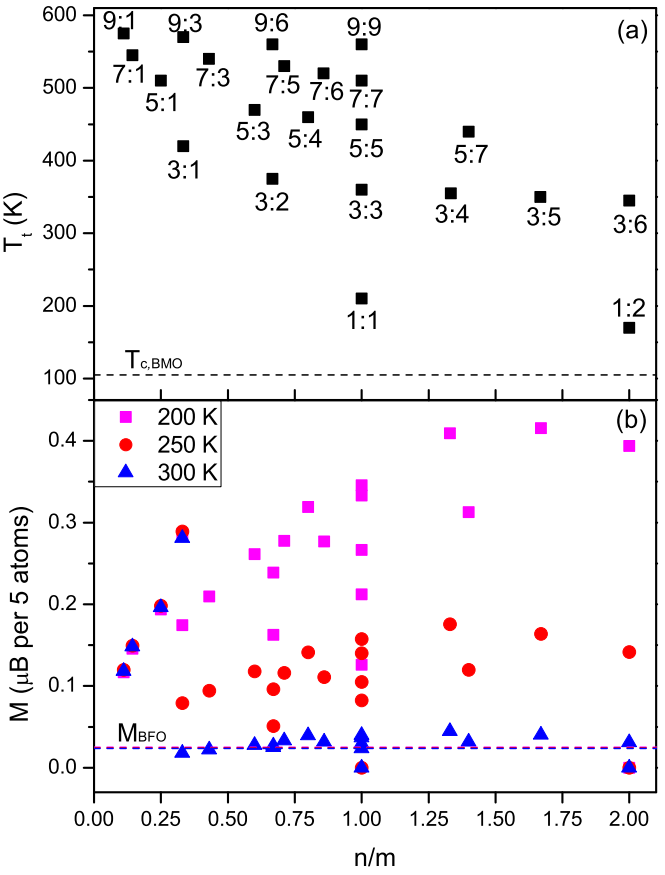

FIG. 3. (Color online) (a) Computed magnetic ordering temperatures for the set of superlattices studied at the level of the spin model in Eq. (1). The results are ordered according to the ratio n/m for each $(BFO)_m$:$(BMO)_n$ SL with m:n shown in the panel. (b) Computed magnetization at three different temperatures, for the same superlattices as shown in (a). The horizontal dashed line in (a) and (b) shows the Curie temperature of pure BMO bulk and the magnetization of BFO thin film, respectively, for comparison.

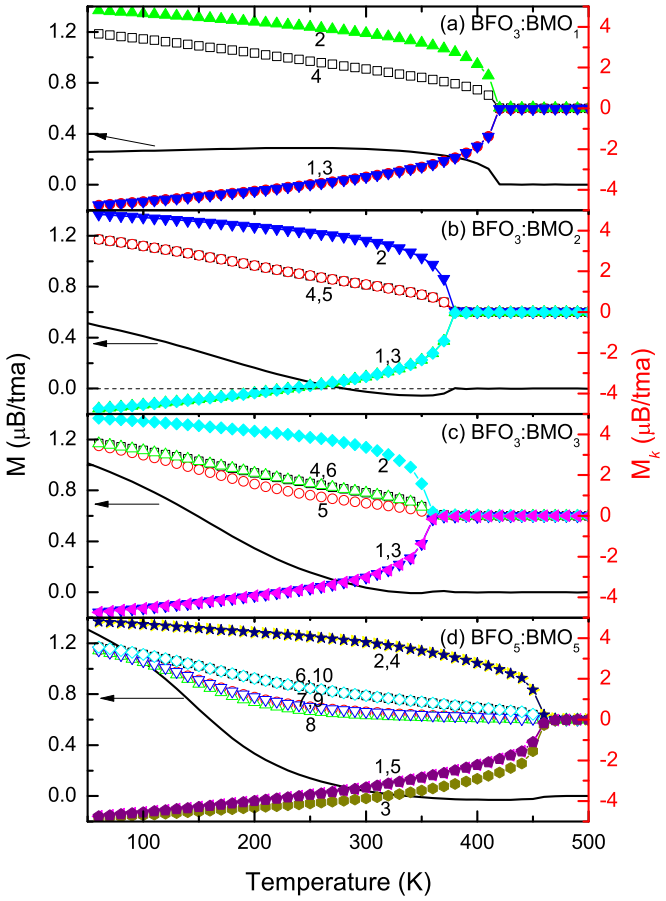

FIG. 4. (Color online) Computed temperature dependence of the total (solid line, using the left axis) and plane-resolved (symbols, using the right axis) magnetizations, for a number of representative superlattices. The solid and open symbols refer to BFO and BMO layers, respectively. For each symbol line we indicate the corresponding layer number.

obtain $M(200\ \mathrm{K}) \approx 0.4\mu_B$ per transition metal atom (μ_B/tma in the following), which is about 40 times that of BFO thin films; unfortunately, the magnetization decays very rapidly when temperature approach T_{room}, reaching values of about $0.02\mu_B$/tma that are comparable to the magnitude of the canted moment in BFO thin films [5–7]. In contrast, we find cases in which $M(T)$ is constant in the T range considered, presenting sizable values between $\simeq 0.1\mu_B$/tma and $\simeq 0.3\mu_B$/tma at T_{room}, which is about one order of magnitude larger than that of BFO films. Interestingly, these are cases in which the BMO layers are very thin, namely, with $n = 1$. How can we explain these counterintuitive results, with the SLs with the smallest fraction of FM material presenting the largest magnetizations at T_{room}?

To get further insight into the magnetic behavior of our SLs, in Fig. 4 we plot the T dependence of the total magnetization $M(T)$, as well as the analogous results for the magnetization $M_k(T)$ of the kth $(111)_{pc}$ plane along z, for a few representative SLs. Many interesting features are obvious from these results: (1) In some cases, we have a nonmonotonic behavior of $M(T)$, which becomes nonzero at T_t and changes sign as we further cool down (see, e.g., the 3:2 case). (2) The alternating positive and negative values of M_k inside the BFO layers reflect the G-AFM order. (3) The BMO layers present a FM order, with a magnetization that aligns antiparallel to the magnetization of the boundary planes of the BFO layer. (4) The onset of magnetic order at T_t is dominated by the planes at the core of the BFO layers; in contrast, the magnetic order in the interfacial BFO planes is comparatively weak [see, e.g., the 5:5 case in Fig. 4(d)]. (5) At T_t, when the BFO layers order, the interfacial BMO planes present a nonzero magnetization as well. For the SLs with very thin BMO layers (e.g., see the 3:1 and 3:2 cases in Fig. 4), the magnetization of the BMO planes displays a temperature dependence that closely resembles the one observed for the BFO planes, and we can say that the SL transforms at T_t as a whole. In contrast, for thicker BMO layers [e.g., the 5:5 case in Fig. 4(d)], the magnetization of the interfacial BMO planes displays a behavior below T_t that is nearly linear and qualitatively different from that of the BFO planes. This order is merely caused by the interfacial exchange-bias field, and is not accompanied by a transformation in the bulk of the BMO layer. In fact, in such cases we find that the BMO layer undergoes a smooth FM transition (typical of a

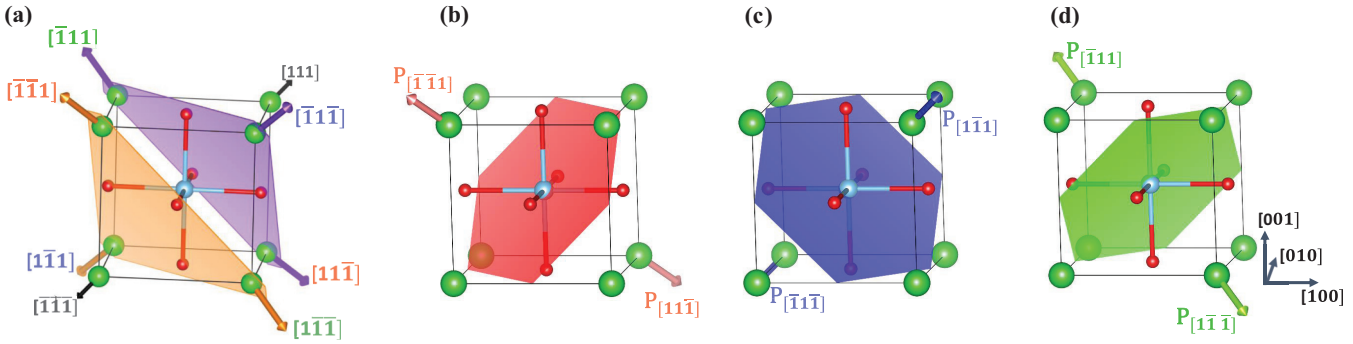

FIG. 5. (Color online) (a) Schematic representation of the possible polarization orientations for a perovskite superlattice grown along the $[111]_{pc}$ direction. The oblique polarization directions are colored purple or orange, respectively, depending on whether they point up (i.e., positive projection along $[111]_{pc}$) or down (i.e., positive projection along $[\bar{1}\bar{1}\bar{1}]_{pc}$). (b), (c), and (d) Schematic diagram of the easy magnetic plane for the state with a polarization oriented along $\pm[11\bar{1}]_{pc}$, $\pm[1\bar{1}1]_{pc}$, and $\pm[\bar{1}11]_{pc}$, respectively.

material under an applied field) at a second critical temperature T_t' that is about 200 K in the 5:5 case shown in Fig. 4(d).

Let us now discuss the behavior of $M(T)$. Note that, for our SLs with odd m, the analytic solution for the ground-state magnetization is

$$M(T \to 0\ \mathrm{K}) = \frac{4n-5}{m+n}\ \mu_B/\mathrm{tma}\ . \qquad (2)$$

This implies that the low-T magnetization of SLs with relatively thick BMO layers ($n \geqslant 3$) will be clearly dominated by the contribution from the Mn cations. However, the situation for such thick-BMO SLs is less clear as T increases. Note that, because the number of BFO planes m is odd in our SLs, the BFO layers present a nonzero net magnetization below T_t, as the G-AFM order is truncated in a way that does not allow for a perfect compensation. [These uncompensated iron spins result in the -5 term in the numerator of Eq. (2).] For T close to T_t, when the order in the BFO layers is strong while the thick BMO layers remain essentially disordered, we find that $M(T)$ is dominated by the BFO contribution. Hence, we naturally obtain the nonmonotonic behavior for $M(T)$ for the 5:5 and 3:3 cases shown in Fig. 4. Accordingly, we expect these SLs with thick BMO layers to present a strong T dependence of the magnetization; this is indeed what we find in the cases with a large n/m ratio mentioned above in connection with the results in Fig. 3.

In contrast, Eq. (2) tells us that the situation for $n = 1$ in $(BFO)_m$:$(BMO)_n$ is very different, as in this case the ground-state magnetization is dominated by the BFO contribution. Hence, as shown in Fig. 3(a), we get a monotonic behavior for $M(T)$, which is weakly T dependent except in the neighborhood of T_t. Note that the best performing SLs shown in Fig. 3(b), which display large $M(T_{room})$ and nearly constant magnetization in the interval between 200 and 300 K, correspond exactly to small n/m ratios with $n = 1$.

IV. DISCUSSION

A. Magnetoelectric effects

Because of their reduced symmetry, our SLs will most likely display a linear magnetoelectric (ME) response, of the type that is known to be very large for materials that are electrically or magnetically *soft*, i.e., that display large dielectric or magnetic susceptibilities [34–36]. In this sense, note that our SLs offer the ideal conditions to enhance such a softness, e.g. by changing the n/m ratio to control the magnetic and FE ordering temperatures.

Furthermore, our BFO:BMO SLs should allow us to obtain a large ME effect associated with the switching between equivalent FE states. As mentioned above, the ground state of our SLs corresponds to having a polarization $\boldsymbol{P}$ oblique to the growth direction z, with six symmetry-equivalent variants being accessible in principle, as shown in Fig. 5(a). More specifically, $\boldsymbol{P}$ can lie (anti)parallel to three distinct crystallographic axes, given by $[\bar{1}11]_{pc}$, $[1\bar{1}1]_{pc}$, and $[11\bar{1}]_{pc}$. From previous studies of BFO's MEM phase, we know that the G-AFM order parameter lies in a plane perpendicular to the polarization direction [see Figs. 5(b)–5(d)], and such a plane changes when an electric field is used to make $\boldsymbol{P}$ switch between equivalent polar states [7,37,38]. In our SLs, the polarization should be easily switchable by 109° between the three oblique states associated with the orange (or purple) colored arrows in Fig. 5(a) by *in-plane* electric fields using planar electrodes as in Ref. [39]. On the other hand, a switch between any of the three "orange states" to any of the three "purple states," or vice versa, would likely require the combination of out-of-plane and in-plane electric fields via the use of both perpendicular and planar electrodes. An analogous electric-field-driven switch between oblique-$\boldsymbol{P}$ states would automatically result in a different orientation of $M(T)$, as shown in Figs. 5(b)–5(d). Our best SLs would thus provide us with a T_{room} magnetization of up to $0.3\mu_B$/tma (more than ten times larger than that of BFO thin films) whose direction is also controllable with an applied electric field.

B. Connections with prior proposals

Interestingly, our solutions with $n = 1$ are reminiscent of a decade-old idea to obtain optimum MEM materials, namely, to consider rocksalt-ordered double perovskites (such as Bi_2FeCrO_6 in the original work of Baettig and Spaldin [16]) in which the AFM interaction between the first-nearest-neighboring magnetic cations (Fe and Cr in Ref. [16])

would lead to a *ferrimagnetic* configuration with a sizable magnetic moment. Unfortunately, such double perovskites tend to display relatively weak magnetic interactions, which renders an ordering temperature below T_{room} and makes them impractical for applications. In our case, our SLs correspond to the double-perovskite order for $m = n = 1$, for which we obtain $T_t = 210$ K. In a sense, the identified optimum SLs with $n = 1$ can be viewed as displaying a quasiferrimagnetic spin arrangement, as incomplete compensation is the origin of their net magnetization. However, in our case, by increasing m with respect to the $m = n = 1$ double-perovskite limit, we achieve a transition temperature above T_{room}.

C. Possible improvements

Let us know discuss how variations in the behavior of the FM layer, and the interfacial coupling, may affect the performance of our SLs at room temperature. For example, let us artificially increase the J_{MnMn} exchange constant so that T_C^{bulk} of the FM layer becomes 275 K. In that case, we obtain an enhanced $M(T_{room})$ of $0.50\mu_B$/tma for the 3:3 case and $0.71\mu_B$/tma for the 5:5 case. Alternatively, if we vary the J_{MnMn} exchange constant so that it has the same magnitude as the one computed but the opposite sign (i.e., rendering a FM coupling between layers), we obtain large $M(T_{room})$ values of $1.24\mu_B$/tma for the 3:1 case, $0.93\mu_B$/tma for the 3:3 case, and $0.63\mu_B$/tma for the 5:5 case. Hence, we find that suitable replacements for BMO in the considered SLs may dramatically increase the values of $M(T_{room})$. Examples of such replacements may be La_2MnNiO_6 ($T_C = 275$ K) [11,12] and Bi_2NiReO_6 ($T_C = 360$ K) [15].

V. CONCLUSIONS

Our results show that our design concept works: We studied $BiFeO_3$:$BiMnO_3$ bicolor superlattices in which, by taking advantage of the strong AFM interactions of $BiFeO_3$, we are able to obtain an ideal MEM material that (1) presents robust and large ME effects at room temperature and (2) offers great freedom to tune its properties to address specific needs. Our results also suggest there is room for further improvement. For example, if we were able to replace $BiMnO_3$ by a compound with a higher Curie temperature, or presenting a FM interfacial interaction with $BiFeO_3$, the values of $M(T_{room})$ might drastically increase. We thus hope our results will encourage experimental work on the investigated superlattices and other nanostructures realizing the same design concept, which appears as a promising path to achieving technologically relevant multiferroics.

ACKNOWLEDGMENTS

Y.Y. and L.B. thank ONR Grant No. N00014-12-1-1034. J.Í. got financial support from MINECO-Spain (Grant No. MAT2013-40581-P).

[1] N. A. Hill, J. Phys. Chem. B **104**, 6694 (2000).
[2] A. Filippetti and N. A. Hill, Phys. Rev. B **65**, 195120 (2002).
[3] S. Bhattacharjee, E. Bousquet, and P. Ghosez, Phys. Rev. Lett. **102**, 117602 (2009).
[4] G. Catalan and J. F. Scott, Adv. Mater. **21**, 2463 (2009).
[5] F. Bai, J. Wang, M. Wuttig, J. Li, N. Wang, A. P. Pyatakov, A. K. Zvezdin, L. E. Cross, and D. Viehland, Appl. Phys. Lett. **86**, 032511 (2005).
[6] H. Béa, M. Bibes, A. Barthélémy, K. Bouzehouane, E. Jacquet, A. Khodan, J.-P. Contour, S. Fusil, F. Wyczisk, A. Forget, D. Lebeugle, D. Colson, and M. Viret, Appl. Phys. Lett. **87**, 072508 (2005).
[7] D. Albrecht, S. Lisenkov, W. Ren, D. Rahmedov, I. A. Kornev, and L. Bellaiche, Phys. Rev. B **81**, 140401 (2010).
[8] I. Sosnowska, T. P. Neumaier, and E. Steichele, J. Phys. C **15**, 4835 (1982).
[9] J. Goodenough, *Magnetism and The Chemical Bond*, Interscience Monographs on Chemistry: Inorganic Chemistry Section (Interscience, New York, 1963).
[10] A. M. D. Santos, S. Parashar, A. Raju, Y. Zhao, A. Cheetham, and C. Rao, Solid State Commun. **122**, 49 (2002).
[11] N. Y. Vasanthacharya, P. Ganguly, J. B. Goodenough, and C. N. R. Rao, J. Phys. C **17**, 2745 (1984).
[12] R. I. Dass, J.-Q. Yan, and J. B. Goodenough, Phys. Rev. B **68**, 064415 (2003).
[13] A. A. Belik, S. Iikubo, T. Yokosawa, K. Kodama, N. Igawa, S. Shamoto, M. Azuma, M. Takano, K. Kimoto, Y. Matsui, and E. Takayama-Muromachi, J. Am. Chem. Soc. **129**, 971 (2007).
[14] H. J. Zhao, W. Ren, Y. Yang, J. Íñiguez, X. M. Chen, and L. Bellaiche, Nat. Commun. **5**, 4021 (2014).
[15] M. Ležaić and N. A. Spaldin, Phys. Rev. B **83**, 024410 (2011).
[16] P. Baettig and N. A. Spaldin, Appl. Phys. Lett. **86**, 012505 (2005).
[17] V. Laukhin, V. Skumryev, X. Martí, D. Hrabovsky, F. Sánchez, M. V. García-Cuenca, C. Ferrater, M. Varela, U. Lüders, J. F. Bobo, and J. Fontcuberta, Phys. Rev. Lett. **97**, 227201 (2006).
[18] Y.-H. Chu, L. W. Martin, M. B. Holcomb, M. Gajek, S.-J. Han, Q. He, N. Balke, C.-H. Yang, D. Lee, W. Hu, Q. Zhan, P.-L. Yang, A. Fraile-Rodriguez, A. Scholl, S. X. Wang, and R. Ramesh, Nat. Mater. **7**, 478 (2008).
[19] S. M. Wu, S. A. Cybart, P. Yu, M. D. Rossell, J. X. Zhang, R. Ramesh, and R. C. Dynes, Nat. Mater. **9**, 756 (2010).
[20] U. Gradmann, J. Magn. Magn. Mater. **6**, 173 (1977).
[21] K. Lenz, S. Zander, and W. Kuch, Phys. Rev. Lett. **98**, 237201 (2007).
[22] D. G. Schlom, L.-Q. Chen, C.-B. Eom, K. M. Rabe, S. K. Streiffer, and J.-M. Triscone, Annu. Rev. Mater. Res. **37**, 589 (2007).
[23] M. Stengel and D. Vanderbilt, Phys. Rev. B **80**, 241103 (2009).
[24] G. Kresse and J. Furthmüller, Phys. Rev. B **54**, 11169 (1996).
[25] G. Kresse and D. Joubert, Phys. Rev. B **59**, 1758 (1999).
[26] S. L. Dudarev, G. A. Botton, S. Y. Savrasov, C. J. Humphreys, and A. P. Sutton, Phys. Rev. B **57**, 1505 (1998).
[27] I. A. Kornev, S. Lisenkov, R. Haumont, B. Dkhil, and L. Bellaiche, Phys. Rev. Lett. **99**, 227602 (2007).
[28] L. Pálová, P. Chandra, and K. M. Rabe, Phys. Rev. Lett. **104**, 037202 (2010).
[29] P. E. Blöchl, Phys. Rev. B **50**, 17953 (1994).
[30] A. Chen, H. Zhou, Z. Bi, Y. Zhu, Z. Luo, A. Bayraktaroglu, J. Phillips, E.-M. Choi, J. L. MacManus-Driscoll, S. J.

Pennycook, J. Narayan, Q. Jia, X. Zhang, and H. Wang, Adv. Mater. **25**, 1028 (2013).

[31] S. Kyun Lee, B. Ho Choi, and D. Hesse, Appl. Phys. Lett. **102**, 242906 (2013).

[32] K. Ujimoto, T. Yoshimura, A. Ashida, and N. Fujimura, Appl. Phys. Lett. **100**, 102901 (2012).

[33] The so-called DFT + U scheme used in this work [26] is reliable to describe magnetism in these insulating oxides at a qualitative level, but is also known to produce J's that fail to reproduce the experimental transition temperatures with quantitative accuracy. To remedy this problem, we rescaled the J's mentioned above following an approach that has previously proven to be very successful [14]. Thus, for example, we considered bulk BFO and, by comparing our computed T_N with the experimental value, deduced a suitable rescaling factor for J_{FeFe} (0.82 in this case); by applying such a rescaling factor to the exchange constant computed for our SLs, we got a value of $J_{FeFe} = 38$ meV, which we then used in the MC simulations. Analogously, we studied BMO's bulk phase and deduced a rescaling factor (0.385) that leads to the value of $J_{MnMn} = -6$ meV used in our MC simulations for the SLs. As for the Mn-Fe coupling, we used an average rescaling factor to obtain $J_{FeMn} = 11.4$ meV.

[34] J. C. Wojdeł and J. Íñiguez, Phys. Rev. Lett. **103**, 267205 (2009).

[35] J. C. Wojdeł and J. Íñiguez, Phys. Rev. Lett. **105**, 037208 (2010).

[36] S. Prosandeev, I. A. Kornev, and L. Bellaiche, Phys. Rev. B **83**, 020102 (2011).

[37] D. Lebeugle, D. Colson, A. Forget, M. Viret, A. M. Bataille, and A. Goukasov, Phys. Rev. Lett. **100**, 227602 (2008).

[38] C. Ederer and N. A. Spaldin, Phys. Rev. B **71**, 060401 (2005).

[39] Z. Chen, X. Zou, W. Ren, L. You, C. Huang, Y. Yang, P. Yang, J. Wang, T. Sritharan, L. Bellaiche, and L. Chen, Phys. Rev. B **86**, 235125 (2012).